High dynamic pressures and modest temperatures: a broad perspective and bridging the gap

2002 J. Phys.: Condens. Matter 14 11045

(http://iopscience.iop.org/0953-8984/14/44/425)

INSTITUTE OF PHYSICS PUBLISHING JOURNAL OF PHYSICS: CONDENSED MATTER

J. Phys.: Condens. Matter **14** (2002) 11045–11054 PII: S0953-8984(02)37327-2

High dynamic pressures and modest temperatures: a broad perspective and bridging the gap

W J Nellis

Lawrence Livermore National Laboratory, University of California, Livermore, CA 94550, USA

Received 22 May 2002
Published 25 October 2002
Online at stacks.iop.org/JPhysCM/14/11045

Abstract
Pressures up to a few 100 GPa and temperatures as high as a few 1000 K have been achieved with high dynamic pressures using a two-stage light-gas gun. Results are reviewed for molecular fluids, metallic hydrogen, solids, implications for planetary interiors, and structures and properties of materials recovered intact from high dynamic pressures.

1. Introduction

Dynamic high pressures are applied rapidly to materials to increase density and temperature, to alter crystal structure and microstructure, and to change physical and chemical properties. Pressures from 1 to 500 GPa (5 Mbar), compressions up to fifteenfold greater than initial liquid density in the case of hydrogen, and temperatures ranging from room temperature up to several electron volts (11 600 K) can be achieved by shock compression of condensed matter. In fact, above 1 GPa the terms shock and dynamic are used interchangeably. At these extreme conditions the bonding, structure, physical, and chemical properties of condensed matter are changed substantially from what they are at ambient. If high-pressure phases can be quenched to ambient, then new opportunities become available in condensed matter and material sciences, as well as potential technological applications. The purpose of this paper is to review results obtained with dynamic high pressures achieved in molecular fluids, metallic hydrogen and solids, discuss implications for giant planets, and describe the structure and properties of materials recovered intact from dynamic high pressures.

2. Molecular fluids and metallic hydrogen

Perhaps the most remarkable observation with this method is metallic fluid hydrogen [1–4]. A metallic state of hydrogen had been sought previously for decades. Those experiments used cryogenic liquid specimens at atmospheric pressure because of the high density of the liquid compared to the gaseous phase. The high initial density of the liquid causes a substantially lower temperature and higher density in the shock-compressed state than if a gaseous sample were used. To enable systematic study of highly compressed fluids, a cryogenic system was

developed to synthesize liquid samples [5, 6] for compression with a two-stage light-gas gun [2]. This cryogenic sample holder enabled investigations of a wide variety of liquids with initial temperatures ranging from 4 to 230 K, including He [7], H_2/D_2 [1–4, 6, 8, 9], N_2 [5, 10–13], O_2 [5, 14, 15], Ar [5], CH_4 [16–18], Xe [19], CO [16], CO_2 [20], and NH_3 [17, 21]. Similar sample holders at room temperature were used to study H_2O [21–24], synthetic Uranus (a mixture of water, ammonia, and isopropanol) [17, 25, 26] and CH_2 and C_6H_6 [18, 27, 28].

Because of the short lifetime of a shock experiment, the compression is adiabatic and temperature increases. The lifetime of a shock state is ∼100 ns for sample dimensions typical of two-stage-gun experiments. This time is more than sufficient to achieve thermal equilibrium in dense fluids. The actual temperature achieved depends sensitively on the number of shocks used to compress to a given pressure. The greater the number of shocks, the lower the temperature and higher the density. High dynamic pressures are generated by impact of a planar impactor onto the sample holder. The impactor is accelerated to velocities in the range 1–8 km s^{-1} with a two-stage light-gas gun. The Hugoniot equation of state (EOS) is the locus of pressure–volume–energy (P–V–E) states achieved by single-shock compression. The three Hugoniot equations are based simply on conservation of momentum, mass, and internal energy across a shock front. Hugoniot points are obtained by measuring impactor velocity and shock velocity, using the previously measured Hugoniot EOSs of the solid impactor and wall of the liquid layer, and using the shock impedance match principle, which states that shock pressure and material velocity are continuous across an interface between two dissimilar materials. Temperature is measured from the optical spectrum emitted from a shock front. Electrical conductivity is measured by inserting electrodes into contact with a shock-compressed sample. Raman spectra are measured by scattering light from a shock-compressed sample. Illustrations of pressure–volume Hugoniot EOS, temperature, and electrical conductivity experiments are shown in figure 1. The impactor launched from the gas gun is incident from the left and electrical or optical signals exit to the right.

One of the most interesting systems observed with these techniques is the continuous dissociative phase transition in dense fluid nitrogen at 30–80 GPa on the Hugoniot [5, 10–12]. This transition causes two unexpected phenomena:

(i) shock-induced cooling, the process in which the temperature of the shock reflected from the anvil, the second shock, is actually lower than the temperature of the shock incident on the anvil, the first shock, and

(ii) temperature decreases with increasing pressure at constant volume.

In the case of nitrogen, item (ii) is indicative of a large negative Grüneisen parameter, which is challenging to understand [29, 30].

The experimental configuration used to measure electrical conductivities of multiply shocked hydrogen and other liquids [1, 13, 15, 24] is illustrated in figure 2. The shock reverberates in the liquid between the two stiff sapphire anvils. This experiment was used to demonstrate that fluid hydrogen achieves the minimum electrical conductivity of a disordered metal at 140 GPa, ninefold compression of the initial liquid density, and 3000 K. The finite temperature produced by dynamic compression causes a disordered liquid which facilitates bridging the mobility gap to achieve a metallic state at a lower pressure than expected for the ordered solid. The metallic state is achieved because pressure reduces the 15 eV gap and thermal disorder fills it in until $E_g/k_B = T \sim 2600$ K, where E_g is smeared out thermally and the electronic system has a Fermi surface ($E_F = 19$ eV). Since $T/T_F \sim 0.01$, metallic hydrogen is highly degenerate. Fluid hydrogen becomes metallic via a continuous transition from semiconductor to metal.

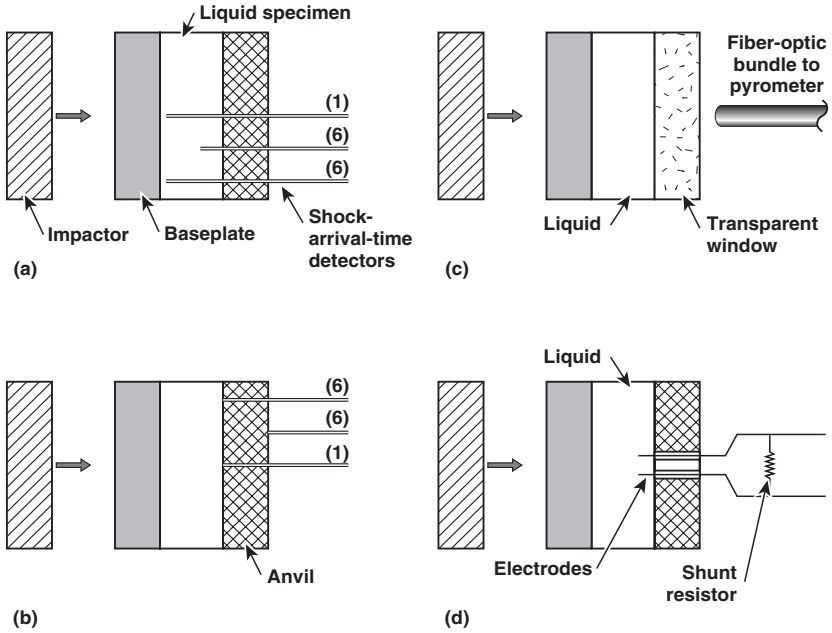

Figure 1. Experimental arrangements in which either the first shock or its reflection from an anvil is diagnosed. (a) Single-shock Hugoniot EOS. The shock velocity is measured in liquid by placing detectors on each of two levels. (b) Double-shock Hugoniot EOS. The shock velocity is measured across the anvil. (c) Shock emission temperatures under single and double shock (the first shock reflects off the window to produce the second shock). (d) Electrical conductivity of singly shocked fluid.

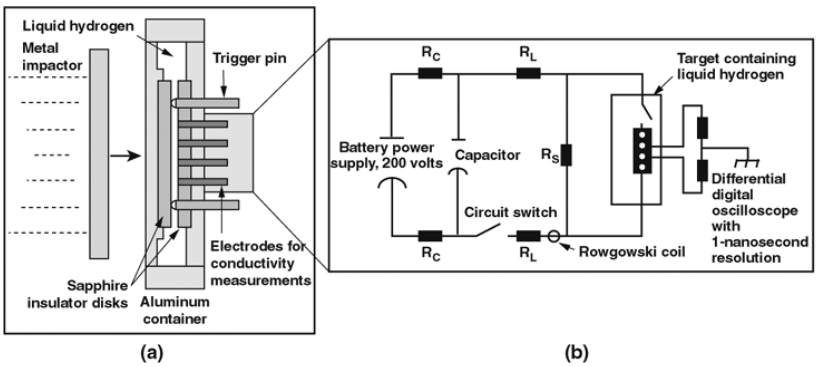

Figure 2. A schematic diagram of the electrical conductivity experiment using a shock wave reverberating between stiff sapphire anvils. Four electrodes in (a) were connected to the circuit in (b). For conductivities lower than metallic, two probes were used. The impactor is accelerated to $\sim$7 km s^{-1} with a two-stage gun [2].

Tight-binding molecular dynamics (MD) [31] show that metallic hydrogen at 3000 K has a peak in the proton–proton pair distribution function at the separation distance between protons in the molecule and that 'molecules' or dimers are short-lived ($\sim 10^{-14}$ s). Kinetic, vibrational, and rotational energies of the transient pairs are comparable. Conduction electrons have a very short mean free path, the distance between adjacent particles ($\sim$2 Å). This is a strong-scattering system characteristic of minimum metallic conductivity.

Fluid Cs, Rb, and H at ∼2000 K metallize with conductivity of 2000 Ω^{-1} cm^{-1} at the same scaled density $D_m^{1/3}a^* = 0.38$, where D_m is the density of atoms at metallization and a^* is the effective Bohr radius [32]. This nonmetal–metal transition is a Mott transition.

The Herzfeld criterion, which depends only on polarization of the atom [33], gives a metallization density of 0.60 mol H cm^{-3}, within 7% of 0.64 mol H cm^{-3} determined by fitting the conductivity data to a thermal activation model in the semiconducting regime and determining the density at which the mobility gap is approximately equal to the thermal energy, $E_g \sim kT$ [2]. At this condition the mobility gap is smeared out thermally and the system has a Fermi surface. This agreement in metallization density between the two methods and the very short dimer lifetimes (∼10^{-14} s) suggest that fluid metallic hydrogen is essentially monomeric.

The metallic conductivity, 2000 Ω^{-1} cm^{-1}, is the minimum conductivity of a metal $\sigma_{min} = 2\pi e^2/(3hd)$, where h is Planck's constant and $d = D_m^{-1/3}$. At the metallization density, 0.60 mol H cm^{-3}, $\sigma_{min} = 6000\ \Omega^{-1}$ cm^{-1}, in good agreement with experiment. Metallic conductivities in good agreement with experiment were calculated with the Ziman model [4] and with tight-binding MD [34]. The latter show that the nonmetal–metal transition in fluid hydrogen is density-driven.

In contrast to the systematic Mott transition to a metallic state in fluid hydrogen [1], oxygen [15], and nitrogen [13], water is a proton conductor at 100 GPa pressures [24].

3. Solids

In order to perform experiments on fluids, it is necessary to know the Hugoniot EOS of the solids used as impactors and as walls of the sample holder. For this reason the Hugoniots of the metals Al, Cu, and Ta were measured up to a few 100 GPa with a two-stage light-gas gun [35]. Higher pressures were measured in various solid specimens using underground nuclear explosives [36–38].

The graphite-to-diamond transition was time-resolved with a velocity interferometer for a surface of any reflector (VISAR) [39, 40]. These experiments showed that the dynamics of this transition is sensitive to the direction of shock propagation with respect to crystallographic orientation and to the microstructure of the sample.

4. Giant planets: experimental constraints

The Jovian planets Jupiter and Saturn together contain over 400 Earth masses, most of which is hydrogen. Pressure and temperature in the mantle of Jupiter range up to a 300 GPa and several 1000 K and are about 4 TPa and 20 000 K at the centre [41]. Hydrogen is fluid at these conditions [42]. Magnetic fields of giant planets are produced by the convective motion of electrically conducting fluid hydrogen by dynamo action [43]. These conditions raise some interesting questions about Jupiter. For example, why is the magnitude of the Jovian magnetic field so large and asymmetric relative to that of Earth and is there a relatively sharp core–mantle boundary in Jupiter between a molecular mantle and monatomic core, analogous to the boundary in the Earth between the rocky mantle and iron core? The most important material to study with respect to the Jovian planets is hydrogen because it has by far the greatest cosmological abundance. The most important materials to study with respect to the 'icy' planets Uranus and Neptune are water, ammonia, methane, and synthetic Uranus, a representative mixture. The purpose of this section is to review the current experimental situation for hydrogen, water, ammonia, methane, and synthetic Uranus and to describe implications for the nature of the interiors of the Jovian and 'icy' planets [44–47].

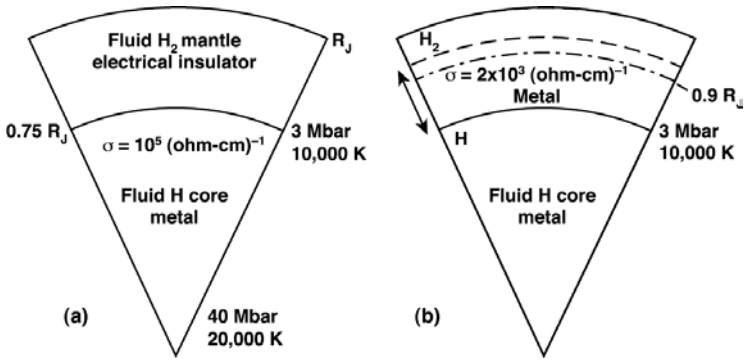

Figure 3. Schematic diagrams of the Jovian interior (a) before and (b) after recent hydrogen experiments at high dynamic pressures and temperatures comparable to those in Jupiter. The 'before' picture in (a) has an insulating molecular mantle which undergoes a transition to a monatomic metallic core via a first-order phase transition at $0.75R_J$. Picture in (b) shows that H_2 is molecular down to ∼40 GPa at $\sim 0.95R_J$, (long-dash curve), at which depth dissociation commences and is completed by $\sim 0.90R_J$ (section 2), where metallization occurs (dot–dash curve). For reference, the solid curve is same as in (a).

The transition from diatomic insulating H_2 to monatomic metallic H at high pressures and temperatures in the fluid has been an important issue in Jovian modelling for decades. Some theoretical work suggested that this transition, often called the plasma phase transition (PPT), is first order [48–50]. Other work suggested that this transition is continuous in pressure and temperature [51]. Since at high shock pressures (>15 GPa) and temperatures, no first-order phase transition has ever been observed in any fluid, it is quite likely that this transition is continuous and, thus, it is most likely that no sharp core–mantle boundary exists in the Jovian planets.

Depending on the model, the radius in Jupiter at which metallization occurs has ranged between 0.75 and 0.90 R_J, where R_J is the radius of Jupiter. We estimated where the Jovian magnetic field is made by estimating where the electrical conductivity of dense fluid hydrogen is large. For purposes of discussion we assume that the path of pressure–temperature (P–T) states in Jupiter is an isentrope. Using a fluid model based on our equation-of-state data, the isentrope of pure hydrogen was calculated from the surface temperature of Jupiter (165 K) [44]. Since He is a small molecule as hydrogen, the equation of state of a mixture containing ∼10 at.% He is not expected to be substantially different from that of pure hydrogen. Temperature rises steeply with increasing pressure (depth in Jupiter) until molecular dissociation begins at ∼40 GPa. At higher pressures up to ∼200 GPa, temperature varies slowly because internal energy is absorbed in dissociation. Electrical conductivity was calculated along the Jovian isentrope using a scaling relationship derived from measured conductivities [45]. Metallization ($2000\ \Omega^{-1}\ \mathrm{cm}^{-1}$) probably occurs in Jupiter at 140 GPa and 4000 K, as it does in our laboratory experiments at 140 GPa and 3000 K, because electrical conductivity is generally slowly varying with temperature in a disordered liquid metal. A pressure of 140 GPa is reached in Jupiter at a radial position of $\sim 0.90R_J$. Assuming that material with a conductivity as low as that in Uranus, $\sim 20\ \Omega^{-1}\ \mathrm{cm}^{-1}$. contributes to the Jovian surface field, then radii out to $\sim 95\%\ R_J$ contribute to the surface magnetic field. The model for Jupiter derived from these considerations is illustrated in figure 3.

Although surface magnetic fields decrease with distance from where they are produced, the Jovian surface magnetic field is probably not significantly lower than where the field is produced because it is generated so close to the surface and, thus, its magnitude is relatively large, ∼10 G. The large asymmetry in the surface magnetic field is also readily observed for the same rea-

son [52]. That is, planetary magnetic fields are typically composed of dipolar and higher-order components. These multipole components are proportional to r^{-n}, where $n = 3, 4, 5, \ldots$. The deeper the magnetic field is produced, the smaller are components of the surface field caused by higher-order multipole components and the more symmetric is the magnetic field.

In contrast with the case for Jupiter, in Saturn the metallic phase of hydrogen is reached at $\sim 0.5 R_S$, where R_S is the radius of Saturn [53], much deeper in the planet than in Jupiter. The equatorial surface magnetic field of Saturn is 0.21 G, substantially smaller than the equatorial surface magnetic field of Jupiter. Thus, the fact that the magnetic field of Jupiter is generated close to the surface and in Saturn it is generated much deeper is consistent with the relative magnitudes of their external magnetic fields.

The planets Uranus and Neptune are thought to have evolved from the accretion of nebular water, ammonia, and methane. At high pressures and temperatures these molecules react chemically to form complex mixtures. The EOSs of these mixtures are responsible for mass distributions and, hence, gravitational moments and their electrical conductivities are responsible for magnetic fields of the icy planets. Water is one of the most studied fluids at high shock pressures. Recent work includes Hugoniot EOS [21], shock temperatures [22], Raman spectroscopy [23], and electrical conductivities [21, 24]. The Hugoniot [21], shock temperatures [17], and electrical conductivities [21] of ammonia have been measured. The Hugoniot EOS [16, 27, 28], shock temperatures [17], and electrical conductivities [18] of methane and other hydrocarbons have been measured. The mixture 'synthetic Uranus' is composed of water, ammonia, and isopropanol in proportions which give near-cosmological abundance ratios of H, O, C, and N. Hugoniot, temperature, and conductivity data have been measured [17, 25, 26, 47]. These data suggest a maximum conductivity of 20 Ω^{-1} cm^{-1} inside the giant icy planets, which is responsible for their magnetic fields, although recent conductivity data for water up to 180 GPa [24] suggests that the maximum conductivity of synthetic Uranus might be 200 Ω^{-1} cm^{-1}.

5. Materials synthesized and recovered from high dynamic pressures

Dynamic high pressures are used to produce novel crystal structures, microstructures, and associated properties by subjecting specimens to dynamic pressures and recovering them intact. Pressure is applied at strain rates up to 10^8 s^{-1} and higher, pressures and temperatures reach as high as 100 GPa (1 Mbar) and a few 1000 K for $\sim\mu$s, and quench at rates up to 10^{12} bar s^{-1} and 10^9 K s^{-1}, as illustrated in figure 4. While pressure releases to zero, temperature releases to a residual value, which is higher than the initial value because of irreversible shock heating. The residual temperature approaches the ambient value by thermal conduction into surrounding material. Such experiments are called recovery experiments. The high quench rates mean that phases and structures synthesized at high shock pressures and temperatures might be quenched to ambient.

The experiments discussed here use a two-stage light-gas gun [54] to accelerate a planar metal projectile to a maximum impactor velocity of $\sim$4 km s^{-1} with He driving gas, which produces 120 GPa for a Cu plate impacting a Cu target. Recovering a sample intact becomes progressively very difficult above 100 GPa. Specimens are typically 10 mm in diameter and 0.001–1 mm thick. Initial temperatures can be varied in the range 100–1300 K [55]. A representative configuration of the fixture which holds a specimen which is shocked and recovered intact is illustrated in figure 5. Some examples of effects produced in materials are described below.

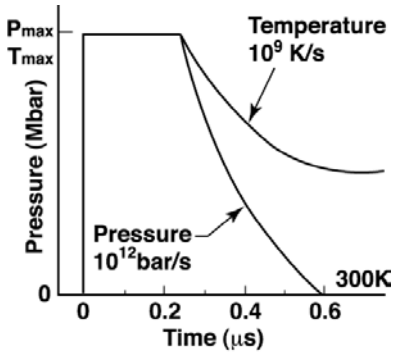

Figure 4. Shock and release profiles calculated in planar geometry for shock-compressed Cu. Pressure releases to zero but temperature does not because of irreversible shock heating.

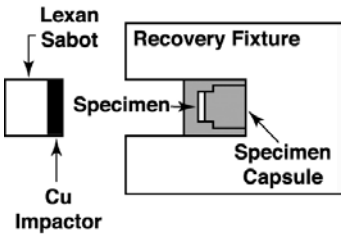

Figure 5. A schematic diagram of an experiment to recover a specimen shocked to pressures up to 100 GPa. The projectile is launched by two-stage light-gas gun [2, 54].

5.1. Nanocrystalline materials

Shock compression of single-crystal quartz causes the formation of polycrystalline grains, which facilitates flow of the bulk sample under rapid deformation at shock pressures of 20–50 GPa. As a result the grain boundaries reach very high heterogeneous temperatures, which reduce SiO_2 to Si and O, which in turn phase separate. Because the duration of maximum pressure in these experiments is a few 100 ns, there is sufficient time only for nanocrystalline Si (n-Si) particles to nucleate and grow *in situ* within the solid SiO_2. These nanoparticles have the well-ordered diamond crystal structure [56]. The size distribution of n-Si can be tuned by choice of shock pressure and its duration. The chemical history of this n-Si is completely different to that of samples made with traditional wet-chemistry methods, which might shed light on the mechanism of their photoluminescence; that is, is photoluminescence caused by quantum confinement or oxygen passivation of the Si surface, and what are the optical effects caused by shock-induced defects?

5.2. Films

High-pressure phases might be synthesized and quenched metastably. Nb films 1–10 μm thick have been recovered from 100 GPa shock pressure [57], demonstrating the feasibility of this process for thin samples with maximum quench rates. This rapid-quenching method might be useful, for example, for quenching metallic fluid hydrogen in a sample one micron thick to a metallic glass at ambient pressure [58]. It has been shown calculationally that pressures ($\sim$140 GPa) and temperatures ($\sim$3000 K) required for hydrogen metallization can be achieved by irradiation with a high-intensity pulsed laser [59].

5.3. Shock-induced defects and flux pinning

Shock deformation induces dislocations and stacking faults, which pin magnetic flux and enhance magnetic hysteresis and magnetic levitation force in superconducting $YBa_2Cu_3O_{7-x}$. Using highly ordered melt-textured specimens and orienting their slip plane at 30° with respect to the shock direction, these brittle oxide specimens can be shocked without macroscopic fracture. After annealing the shocked specimen in oxygen to repair shock-induced damage in bulk, dislocations are converted into stacking faults. As a result the magnetic hysteresis, and thus critical current density, at 1 kOe and 70 K is about 20% greater than the value before shock at 7 GPa [60].

Shock compaction of $SmCo_5$ particles at ∼8 GPa enhances binding forces between particles and induces defects, increasing the 'permanency' of this permanent ferromagnet [61].

5.4. Synthesis of hard materials

Potentially new hard materials can be synthesized and recovered from dynamic high pressures. For example, shock-compressed mixtures of C_{60} fullerenes and Cu powders produce fine-grained diamond [62]. Nanocrystalline metastable diamond films have been produced by shock compression of 2 μm thick C_{60} fullerene films [63].

5.5. Powder consolidation

Dynamic compaction rapidly consolidates powders by depositing compressive energy on particle surfaces, which are heated heterogeneously, often bond together, and then quench thermally to the interiors of the particles forming a dense compact. Advantages include:

(i) focusing energy on particle surfaces so that the whole bulk system does not need to be heated for compaction and
(ii) consolidating powders so quickly that grains do not have time to grow nor do metastable phases have time to decompose.

Single-piece discs of both conventional and rapidly solidified alumina/zirconia ceramics have been consolidated by a reverberating shock wave [64]. A computational model has been developed for dynamic compaction which could be applied to a wide variety of materials, pressures, and consolidation rates and, thus, address key issues computationally [65].

5.6. Shock-induced melting and rapid resolidification

Because powders have a lower initial density than a crystalline solid, powders are more compressible and, thus, have higher internal shock energies and higher shock temperatures at a given volume than do solid specimens. Thus, there is a range of relatively high shock pressures in which powders are readily shock melted in bulk and thermally quenched by thermal conduction into surrounding solid metals such as Cu. At relatively lower shock pressures powders are simply compacted dynamically by a shock as discussed in 5.5. Model calculations were used to predict that Cu–Zr powders would compact at 16 GPa and shock-melt at 60 GPa, as observed by experiment [66].

Acknowledgment

This work was performed under the auspices of US Department of Energy by the University of California Lawrence Livermore National Laboratory under Contract no W-7405-ENG-48.

References

[1] Weir S T, Mitchell A C and Nellis W J 1996 *Phys. Rev. Lett.* **76** 1860
[2] Nellis W J, Weir S T and Mitchell A C 1999 *Phys. Rev.* B **59** 3434
[3] Nellis W J 2000 *Sci. Am.* **84** (May)
[4] Nellis W J, Louis A A and Ashcroft N W 1998 *Phil. Trans. R. Soc.* A **356** 119
[5] Nellis W J and Mitchell A C 1980 *J. Chem. Phys.* **73** 6137
[6] Nellis W J *et al* 1983 *J. Chem. Phys.* **79** 1480
[7] Nellis W J *et al* 1984 *Phys. Rev. Lett.* **53** 1248
[8] Nellis W J *et al* 1992 *Phys. Rev. Lett.* **68** 2937
[9] Holmes N C, Nellis W J and Ross M 1995 *Phys. Rev.* B **52** 15 835
[10] Nellis W J *et al* 1984 *Phys. Rev. Lett.* **53** 1661
[11] Radousky H B *et al* 1986 *Phys. Rev. Lett.* **57** 2419
[12] Nellis W J *et al* 1991 *J. Chem. Phys.* **94** 2244
[13] Chau R, Mitchell A C and Nellis W J 2002 unpublished
[14] Hamilton D C *et al* 1988 *J. Chem. Phys.* **88** 5042
[15] Bastea M, Mitchell A C and Nellis W J 2001 *Phys. Rev. Lett.* **86** 3108
[16] Nellis W J *et al* 1981 *J. Chem. Phys.* **75** 3055
[17] Radousky H B *et al* 1990 *J. Chem. Phys.* **93** 8235
[18] Nellis W J, Hamilton D C and Mitchell A C 2001 *J. Chem. Phys.* **115** 1015
[19] Nellis W J, van Thiel M and Mitchell A C 1982 *Phys. Rev. Lett.* **48** 816
[20] Nellis W J *et al* 1991 *J. Chem. Phys.* **95** 5268
[21] Mitchell A C and Nellis W J 1982 *J. Chem. Phys.* **76** 6273
[22] Lyzenga G A *et al* 1982 *J. Chem. Phys.* **76** 6282
[23] Holmes N C *et al* 1985 *Phys. Rev. Lett.* **55** 2433
[24] Chau R *et al* 2001 *J. Chem. Phys.* **114** 1361
[25] Nellis W J *et al* 1988 *Science* **240** 779
[26] Nellis W J *et al* 1997 *J. Chem. Phys.* **107** 9096
[27] Hamilton D C *et al* 1988 *J. Chem. Phys.* **88** 7706
[28] Nellis W J *et al* 1984 *J. Chem. Phys.* **80** 2789
[29] Ross M 1987 *J. Chem. Phys.* **86** 7110
[30] Mazevet S, Johnson J D, Kress J D, Collins L A and Blottiau P 2002 *Phys. Rev.* B **65** 014204
[31] Lenosky T J *et al* 1997 *Phys. Rev.* B **55** R11 907
[32] Hensel F and Edwards P 1996 *Phys. World* **4** 43
[33] Herzfeld K F 1927 *Phys. Rev.* **29** 701
[34] Kress J *et al* 1998 *Strongly Coupled Coulomb Systems* ed G J Kalman, J M Rommel and K Blagoev (New York: Plenum) pp 331–5
[35] Mitchell A C and Nellis W J 1981 *J. Appl. Phys.* **52** 3363
[36] Nellis W J, Moriarty J A, Mitchell A C, Ross M, Dandrea R G, Ashcroft N W, Holmes N C and Gathers R G 1988 *Phys. Rev. Lett.* **60** 1414
[37] Mitchell A C *et al* 1991 *J. Appl. Phys.* **69** 2981
[38] Nellis W J, Mitchell A C and McMahan A K 2001 *J. Appl. Phys.* **90** 696
[39] Erskine D J and Nellis W J 1991 *Nature* **349** 317
[40] Erskine D J and Nellis W J 1992 *J. Appl. Phys.* **71** 4882
[41] Zharkov V N and Gudkova T V 1992 *High-Pressure Research: Application to Earth and Planetary Sciences* ed Y Syono and M H Manghnani (Tokyo: Terra Scientific) pp 393–401
[42] Ross M, Graboske H C and Nellis W J 1981 *Phil. Trans. R. Soc.* A **303** 303
[43] Stevenson D J 1983 *Rep. Prog. Phys.* **46** 555
[44] Nellis W J, Ross M and Holmes N C 1995 *Science* **269** 1249
[45] Nellis W J, Weir S T and Mitchell A C 1996 *Science* **273** 936
[46] Nellis W J 2000 *J. Planet. Space Sci.* **48** 671
[47] Hubbard W B *et al* 1991 *Science* **253** 648
[48] Stevenson D J and Salpeter E E 1977 *Astrophys. J. Suppl. Ser.* **35** 221
[49] Saumon D and Chabrier G 1992 *Phys. Rev.* A **46** 2084
[50] Magro W R D *et al* 1996 *Phys. Rev. Lett.* **76** 1240
[51] Hubbard W B and Marley M S 1989 *Icarus* **78** 102
[52] Smoluchowski R 1975 *Astrophys. J.* **200** L119
[53] Stevenson D J 1982 *Annu. Rev. Earth Planet. Sci.* **10** 257

[54] Nellis W J 1997 *Encyclopedia of Applied Physics* vol 18 (New York: VCH) p 541
[55] Gratz A J *et al* 1992 *Phys. Chem. Minerals* **19** 267
[56] Fiske P S *et al* 1995 *Science* **270** 281
[57] Koch R, Nellis W J, Hunter J W, Davidson H and Geballe T H 1990 *Pract. Metall.* **27** 391
[58] Nellis W J 1999 *Phil. Mag.* B **79** 655
[59] Pollaine S M and Nellis W J 2000 *Science and Technology of High Pressure* ed M H Manghnani, W J Nellis and M F Nicol (Hyderabad: Universities Press) pp 210–11
[60] Nellis W J *et al* 1994 *High-Pressure Science and Technology—1993* ed S C Schmidt, J W Shaner, G A Samara and M Ross (New York: AIP) pp 695–7
[61] Chau R, Maple M B and Nellis W J 1996 *J. Appl. Phys.* **79** 9236
[62] Sekine T 1992 *Proc. Japan. Acad. Ser.* B **68** 95
[63] Yoo C S *et al* 1992 *Appl. Phys. Lett.* **61** 273
[64] Freim J, McKittrick J and Nellis W J 1994 *High-Pressure Science and Technology—1993* ed S C Schmidt, J W Shaner, G A Samara and M Ross (New York: AIP) pp 1263–6
[65] Benson D J and Nellis W J 1994 *Appl. Phys. Lett.* **65** 418
[66] Nellis W J *et al* 1988 *Shock Waves in Condensed Matter—1987* ed S C Schmidt and N C Holmes (New York: Elsevier) pp 407–10